

The Plasmon Resonance of a Multilayered Gold Nanoshell and its Potential Bioapplications

Changhong Liu, Chris Chunting Mi, *Senior Member, IEEE*, and Ben Q. Li

Abstract—The optical spectra and near-field enhancement of a multilayered gold nanoshell were theoretically studied in this paper to explore its potential biological applications. The mathematical model was developed within the framework of multipole expansion of a multilayered concentric sphere. Results show that compared with a conventional single-layered Au–SiO₂ nanoshell, a multilayered Au–SiO₂–Au nanoshell has an advantage of realizing the localized surface plasmon resonance at wavelength of 1300 nm or longer, which is believed to be more beneficial to ultrahigh resolution optical coherent imaging. With single-layered nanoshell, an extremely thin gold layer is required for resonance at long wavelength, and making such thin layer would be almost practically impossible within the current synthesis techniques.

Index Terms—Field enhancement, gold nanoshell, multilayer, nanoparticle, nanoshell, optical spectra, plasmon resonance.

I. INTRODUCTION

A METALLIC nanoshell, which consists of a dielectric core coated with a thin metallic shell, has attracted considerable attention in recent years due to its favorable optical tunabilities for biomedical imaging and photothermal treatment [1]–[5]. Advances in synthesis techniques make it possible to create nanoparticles with the desired size and structure. By appropriate design of the core-to-shell ratio, the localized surface plasmon resonance (LSPR) effect can be tuned in the spherical metallic nanoshells. This makes these nanoshells agents either for absorbing or scattering light in the region from ultraviolet light to the infrared. The nanoshells with LSPR in the near infrared (NIR) region are well suited for biomedical applications, since the NIR spectrum is almost transparent to most biological tissue [6], [7].

Pioneered by Westcott *et al.*, single-layered Au–silica nanoshells, i.e., a silica core covered by a gold shell, were successfully fabricated ten years ago [8]. Since then, numerous synthesis techniques were developed to produce more controllable shell thickness and homogeneity of the coating [9]–[13]. Besides the work of core–shell particle synthesis techniques, much research was devoted to biological applications. Hirsch *et al.* re-

ported that *in vivo*, exposure to low doses of NIR light (820 nm, 4 W/cm²), solid tumors treated with metal nanoshells reached average maximum temperatures capable of inducing irreversible tissue damage ($\Delta T = 37.4 \pm 6.6$ °C) within 4–6 min [1]. This implies that gold nanoshells can be regarded as a heating carrier for photothermal treatment for cancer. The predominating benefit of nanoshell-based photothermal treatment is that it provides a minimally invasive, however, maximally efficient alternative to conventional clinical treatment of cancers.

Loo *et al.* first described the use of nanoshell-based diagnostic approaches including the development of nanoshell bioconjugates for molecular imaging and the use of scattering nanoshells as contrast agents for optical coherence tomography (OCT) [3]. Afterward, Loo *et al.* demonstrated the application of nanoshell-based techniques for integrating cancer imaging and therapy [4]. This paves the way of dual imaging/heating immunotargeted nanoshells to detect and selectively destroy cancer cells. By using the dual-function-nanoshell techniques in a mouse model, Gobin *et al.* illustrated the dramatic contrast enhancement for OCT and effective photothermal ablation of tumors [5]. OCT, typically employing NIR light, is a novel biomedical optical-imaging technology that produces real time, noncontact, and ultrahigh resolution cross-sectional images of living tissue [14]–[16]. Recent advances in optical material and fabrication techniques have led to micrometer-scale resolution, which is almost ten times as high as conventional ultrasound imaging. The combination of OCT technology and the scattering dominant plasmonic resonance design by tuning the size and shape of gold nanoshell creates a very brilliant future for early tumor detection.

Bioapplications with nanoshells have primarily used laser with ~ 800 nm wavelength, since in that “biological window” (wavelengths ranging from 800 to 1300 nm), attenuation of light is due largely to scattering, rather than absorption. This allows the laser to penetrate more deeply without too much heat absorbed by healthy tissue in the way to access the targeted tumor. The problem is what the best wavelength is in biological window. Imaging experiments, either *ex vivo* or *in vitro*, however, have shown better images by using a laser source with around 1300-nm wavelength. Drexler and coworkers reported that significantly better image penetration depth can be achieved with light centered at 1350 nm than at 850 nm [15]. It has been believed that the optimum wavelength for imaging in biological tissues is in the 1300–1500-nm range [16]–[18] due to the relatively deeper laser penetration in tissue.

To achieve a red-shifted resonance wavelength, one of the measures is to increase the refractive index of the dielectric core [19]. Unfortunately, such tunability of resonance is very limited. With refractive index of core changing from 1.45 to

Manuscript received December 31, 2009; accepted September 14, 2010. Date of publication September 23, 2010; date of current version July 8, 2011. The review of this paper was arranged by Associate Editor D. Hammerstrom.

C. Liu is with Key Laboratory of Control of Power Transmission and Conversion, Ministry of Education, Department of Electrical Engineering, Shanghai Jiao Tong University, Shanghai 200240, China (e-mail: liuch@sjtu.edu.cn).

C. C. Mi is with Department of Electrical and Computer Engineering, University of Michigan-Dearborn, MI 48128 USA (e-mail: chrismi@umich.edu).

B. Q. Li is with Department of Mechanical Engineering, University of Michigan-Dearborn, MI 48128 USA (e-mail: benqli@umich.edu).

Color versions of one or more of the figures in this paper are available online at <http://ieeexplore.ieee.org>.

Digital Object Identifier 10.1109/TNANO.2010.2079943

2.45, the resonance peak shifts only 110 nm toward red. With the development of new technology and new material, it would be possible to produce any kind of materials with the desired optical properties. However, any material implanted into human body must be safe, stable, and biologically and physiologically compatible. Meanwhile, long-term tests and observations are unavoidable before real clinical applications are made.

Another measure to obtain a longer resonance wavelength is to increase the core-to-shell ratio of Au–silica nanoshell [20], i.e., to decrease the shell thickness while keeping the core size constant. Theoretically, the resonance peak can be arbitrarily tuned in the NIR. The difficulty lies in the fact that it is hard to coat a uniform metal layer with thickness less than 10 nm with current synthesis techniques. As an alternative, core size and shell thickness can be increased simultaneously, while keeping the same core-to-shell ratio. However, a larger particle becomes predominantly scattering, rather than absorption, and the line width of spectra curve become broadened, making them less attractive for bioimaging [21].

In this paper, we present an alternative way to achieve longer wavelength plasmon resonance using a multilayered nanoshell. With reasonable structure design and giving consideration to current fabrication techniques, plasmon resonance peak will appear in the region as far as 1200–1300 nm. Moreover, the ratio of absorption and scattering in the total extinction is controllable. The overall particle size is still comparable to the conventional nanoshell. It should be stated that all the geometry sizes of particles discussed in this paper are based on those, which have been reported successfully synthesized in a laboratory environment [9]–[13].

In the following sections, we first present the electromagnetic (EM) model and an efficient recursive calculation method used for a nanoshell with arbitrarily layers. Then, the variation of spectra with physical parameters will be discussed. The near-field enhancements caused by surface plasmon resonance in a multilayered nanoshell will be compared to that in conventional nanoshell to reveal the nature of the LSPR of a multilayered nanoshell.

II. METHODOLOGY

A. Light Scattering and Absorption by a Multilayered Sphere

The EM-scattering theory of a coated concentric sphere was studied in 1951 [22]. Since then, many computation algorithms have appeared with improved computational efficiency [23]–[26]. Among these references, the code given by Bohren and Huffman might be the most popular one to describe a concentric coated sphere. For a conventional single-layer sphere (e.g., Au–silica nanoshell), the calculation procedure is straightforward. By matching boundary conditions at two interfaces, the eight coefficients related to EM vectors can be determined, and then the EM field of everywhere is accordingly obtained. In theory, this procedure can be employed to study a multilayered particle. However, with the number of layer increasing, the solution can be very complex. A concise recursive method was first proposed by Wu and Wang [27], and improved by Wu and

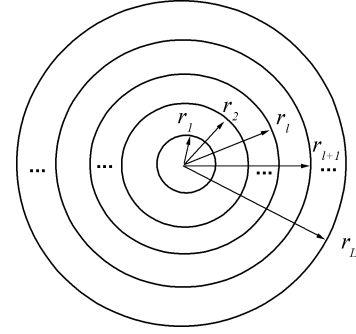


Fig. 1. Geometry of a multilayered sphere.

Wang [27] and Yang [28]. In this paper, a modified algorithm based on Yang's formula will be used.

Fig. 1 shows a spherical particle with L -layer illuminated by an x -polarized plane wave along z -direction. Each layer of the particle is characterized by a size parameter $x_l = 2\pi N r_l / \lambda$ and a relative refractive index $m_l = N_l / N$, where λ is wavelength, r_l and N_l are radius and refractive index of the l th layer ($l = 1, 2, \dots, L$), and N is refractive index of the host media. By means of spherical eigenvectors, the EM field inside the l th layer can be expanded as follows:

$$\mathbf{E}_l = \sum_{n=1}^{\infty} E_n [c_n^l \mathbf{M}_{o1n}^{(1)} - i d_n^l \mathbf{N}_{e1n}^{(1)} + i a_n^l \mathbf{N}_{e1n}^{(3)} - b_n^l \mathbf{M}_{o1n}^{(3)}] \quad (1)$$

$$\mathbf{H}_l = -\frac{k_l}{\omega \mu} \sum_{n=1}^{\infty} E_n [d_n^l \mathbf{M}_{e1n}^{(1)} + i c_n^l \mathbf{N}_{o1n}^{(1)} - i b_n^l \mathbf{N}_{o1n}^{(3)} - b_n^l \mathbf{M}_{e1n}^{(3)}] \quad (2)$$

where $E_n = i^n E_0 (2n + 1) / n(n + 1)$, and superscript (1) and (3) of the vector harmonic functions correspond to Bessel function and Hankel function, respectively.

At each interface, the tangential components of vectors \mathbf{E} and \mathbf{H} are continuous

$$(\mathbf{E}_{l+1} - \mathbf{E}_l) \times \hat{\mathbf{e}}_r = 0, \quad (\mathbf{H}_{l+1} - \mathbf{H}_l) \times \hat{\mathbf{e}}_r = 0. \quad (3)$$

Substituting (1) and (2) to (3) yield four linear equations as follows:

$$\begin{aligned} & d_n^{l+1} m_l \psi_n'(m_{l+1} x_l) - a_n^{l+1} m_l \zeta_n'(m_{l+1} x_l) \\ & - d_n^l m_{l+1} \psi_n'(m_l x_l) + a_n^l m_{l+1} \zeta_n'(m_l x_l) = 0 \\ & c_n^{l+1} m_l \psi_n(m_{l+1} x_l) - b_n^{l+1} m_l \zeta_n(m_{l+1} x_l) \\ & - c_n^l m_{l+1} \psi_n(m_l x_l) + b_n^l m_{l+1} \zeta_n(m_l x_l) = 0 \\ & d_n^{l+1} \psi_n'(m_{l+1} x_l) - b_n^{l+1} \zeta_n'(m_{l+1} x_l) \\ & - c_n^l \psi_n'(m_l x_l) + b_n^l m_{l+1} \zeta_n'(m_l x_l) = 0 \\ & d_n^{l+1} \psi_n(m_{l+1} x_l) - a_n^{l+1} \zeta_n(m_{l+1} x_l) \\ & - d_n^l \psi_n(m_l x_l) + a_n^l \zeta_n(m_l x_l) = 0 \end{aligned} \quad (4)$$

where $\psi_n(z)$ and $\zeta_n(z)$ are the Riccati–Bessel functions.

From (4), coefficients c and d can be derived as follows:

$$\begin{aligned} d_n^l &= d_n^{l+1} \frac{\psi_n(m_{l+1}x_l) - A_n^{l+1}\zeta_n(m_{l+1}x_l)}{\psi_n(m_lx_l) - A_n^l\zeta_n(m_lx_l)} \\ c_n^l &= c_n^{l+1} \frac{m_l}{m_{l+1}} \frac{\psi_n(m_{l+1}x_l) - B_n^{l+1}\zeta_n(m_{l+1}x_l)}{\psi_n(m_lx_l) - B_n^l\zeta_n(m_lx_l)} \end{aligned} \quad (5)$$

where

$$A_n^l = \frac{a_n^l}{d_n^l}, \quad B_n^l = \frac{b_n^l}{c_n^l}. \quad (6)$$

To determine the coefficients d_n^l and c_n^l , we first work out A_n^l and B_n^l ($l = 1, 2, \dots, L + 1$) by a recursion method, which starts from the innermost layer ($l = 1$)

$$A_n^1 = B_n^1 = 0$$

$$H_n^a(m_1x_1) = H_n^b(m_1x_1) = D_n^{(1)}(m_1x_1)$$

$$H_n^a(m_lx_l) = \frac{R_n(m_lx_l)D_n^{(1)}(m_lx_l) - A_n^l D_n^{(3)}(m_lx_l)}{R_n(m_lx_l) - A_n^l}$$

$$H_n^b(m_lx_l) = \frac{R_n(m_lx_l)D_n^{(1)}(m_lx_l) - B_n^l D_n^{(3)}(m_lx_l)}{R_n(m_lx_l) - A_n^l} \quad (7)$$

$$A_n^{l+1} = R_n(m_{l+1}x_l) \frac{m_{l+1}H_n^a(m_lx_l) - m_l D_n^{(1)}(m_{l+1}x_l)}{m_{l+1}H_n^a(m_lx_l) - m_l D_n^{(3)}(m_{l+1}x_l)}$$

$$B_n^{l+1} = R_n(m_{l+1}x_l) \frac{m_l H_n^b(m_lx_l) - m_{l+1} D_n^{(1)}(m_{l+1}x_l)}{m_l H_n^b(m_lx_l) - m_{l+1} D_n^{(3)}(m_{l+1}x_l)}$$

with $D_n^{(1)}(z) = \psi_n'(z)/\psi_n(z)$, $D_n^{(3)}(z) = \zeta_n'(z)/\zeta_n(z)$, and $R_n(z) = \psi_n(z)/\zeta_n(z)$.

To this point, d_n^l , c_n^l , a_n^l , and b_n^l of the l th layer are all obtained. Therefore, the solution to (1) is worked out.

The overall scattering properties of a multilayered particle are then given by the usual expressions

$$\begin{aligned} Q_{sca} &= \frac{2\pi}{x_L^2} \sum_{n=1}^{\infty} (2n+1) (|a_n^{L+1}|^2 + |b_n^{L+1}|^2) \\ Q_{abs} &= \frac{2\pi}{x_L^2} \sum_{n=1}^{\infty} (2n+1) \text{Re}[a_n^{L+1} + b_n^{L+1}]. \end{aligned} \quad (8)$$

B. Intrinsic Size Effect

The optical properties of gold used in this paper were obtained from Johnson and Christy [29], and modified in view of intrinsic size effect. With size effect included, the damping constant is given by

$$\Gamma = \Gamma_{\text{bulk}} + \frac{A v_f}{r} \quad (9)$$

where Γ_{bulk} is the damping constant for the bulk gold, v_f is the Fermi velocity, r is shell thickness, and A is empirical constant

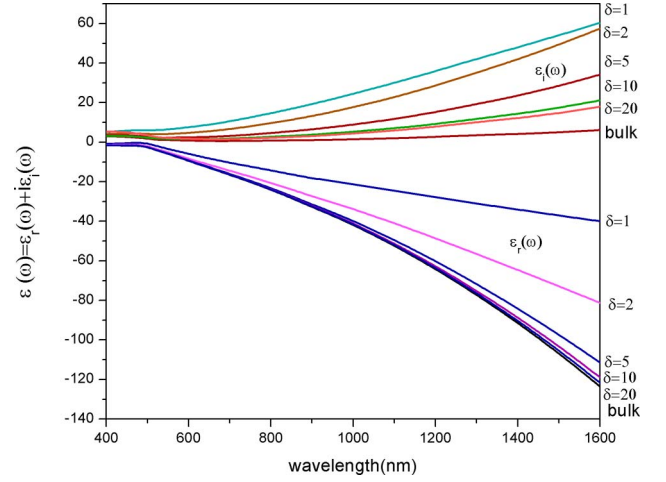


Fig. 2. Size effect on dielectric functions of gold. The upper six curves are the imaginary part with layer thickness δ of 1, 2, 5, 10, and 20 nm, and bulk volume gold; the lower six curves are their real parts.

depending on particle shape and size [29], [30]. In this paper, A is assigned as unity. In the light of size effect modification, the dispersive dielectric function is

$$\varepsilon(\omega) = \varepsilon_{\text{exp}}(\omega) + \frac{\omega_p^2}{\omega^2 + i\gamma_{\text{bulk}}\omega} - \frac{\omega_p^2}{\omega^2 + i\gamma\omega} \quad (10)$$

where $\varepsilon_{\text{exp}}(\omega)$ is the experimental value of bulk gold, ω_p is the bulk plasma frequency, and γ_{bulk} is the bulk scattering rate. In the simulation, $\omega_p = 13.8 \times 10^{15} \text{ s}^{-1}$, $\gamma_{\text{bulk}} = 0.105 \times 10^{15} \text{ s}^{-1}$, and $v_f = 1.39 \times 10^6 \text{ m/s}$.

Fig. 2 is the dispersive curve with size effect. It can be seen that with the increasing of shell thickness, the real part and imaginary part of the dielectric function are getting closer to the bulk curve. At a thickness of 20 nm, the real part is much closed to that without considering size effect. This is verified by Nehl *et al.* [30].

C. Verification

The algorithm of a multilayered sphere described in the previous section was first validated against the experimental result of individual Au-silica nanoshell presented by Nehl. In the calculation, the core and shell size is 60-nm radius and 20-nm thick, respectively. The particle was assumed surrounded by water, and the refractive index of water and silica was set to 1.33 and 1.45, respectively, independent with wavelengths. Empirical constant A is set to 1. As is evident in Fig. 3, the data from theoretical modeling compare reasonably well with the measured data.

III. RESULTS AND ANALYSIS

A. Spectra Properties of a Conventional Nanoshell

In order to shift the resonance to a longer wavelength region, the effect of the refractive index of dielectric core, which is denoted by n_1 , to the optical spectra, was first examined. In Fig. 4, a nanoshell with 60-nm radius dielectric core and 12-nm gold-shell thickness was used as an example. This particle size is very similar to that adopted by Gobin, with 59.5- and 71.5-nm

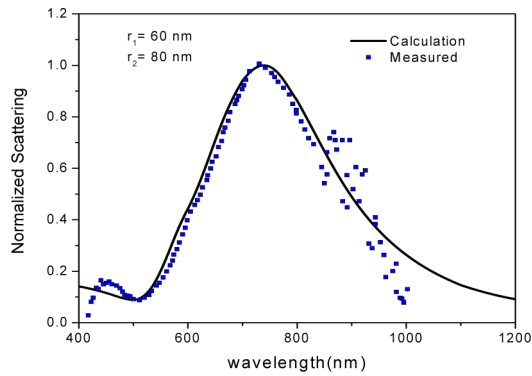


Fig. 3. Verification of calculated normalized scattering spectra of an Au-silica nanoshell. The inner and outer radii were indicated in the figure. The solid line is obtained by the recursive calculation described in this paper, and the dotted points are measured results, taken from [30].

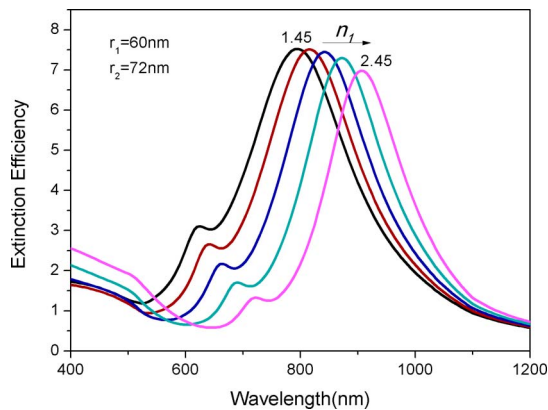


Fig. 4. Extinction efficiency of Au-SiO₂ nanoshell. The inner and outer radii are indicated in the figure. The surrounding medium is water. The curves from left to right correspond refractive index of the core is 1.45, 1.70, 1.95, 2.20, and 2.45, respectively.

inner and outer radii. Since the optical property of most biotissue is very close to water, the surrounding environment is fixed as water. It can be seen from Fig. 4 that with the increasing of refractive index of core, the resonance shifts toward red. With n_1 increasing from 1.45 (SiO₂) to 2.45, the peak moves 110 nm, from 795 to 905 nm. Clearly, for resonance to occur at 1300 nm or even higher, the core would need a much larger refractive index. A biocompatible dielectric with thus high refractive index is yet to be found.

The second choice to tune the resonance, probably the most accessible one, is to decrease the metal layer thickness. Fig. 5(a) shows the resonance red shift by tuning the shell thickness. With SiO₂ core radius fixed at 60 nm, the thickness of gold shell varies from 16 to 4 nm. The corresponding peak appears at 755, 795, 880, and 1085 nm, respectively. Obviously, to obtain resonance around 1300 nm, the shell thickness should be smaller than 4 nm. According to literature, such thin gold layer is extremely difficult, if not possible at all, to realize by current synthesis techniques. An improved alternative is to increase both SiO₂ and gold shell. As indicated in Fig. 5(b), an enlarged nanoshell with applicable 12-nm gold layer presents a red-shifted peak at

1130 nm. However, the spectra curves are dramatically broadened, which is undesirable for high-resolution imaging [21].

B. Spectra Properties of an Au-SiO₂-Au Nanoshell

Compared to the conventional Au-SiO₂ nanoshell, there are three layers in an Au-SiO₂-Au particle. This is equivalent to embedding an addition gold nanoparticle in the sphere center of a SiO₂ particle. Fig. 6 shows the spectra variation with a gold core. Fig. 6(a)-(f) correspond to core radius of 0, 30, 40, 45, 50, and 55 nm. When $r_1 = 0$, a three-layer nanoshell degenerates to a conventional Au-SiO₂ nanoshell.

As appears in Fig. 6, there are two dipole resonance peaks in the visible (VIS) and NIR region. Since the resonance of a solid gold particle occurs in the region from 525 to 600 nm, the left peak is contributed by the gold core, and the right one by the gold shell. With the gold core increasing in size, the first (or left) peak becomes more pronounced, and eventually becomes dominant. Notice that the position of the left peak shifts slightly toward red when the gold core size gradually increases. This is consistent with that of an insulated gold particle.

In Fig. 6, it is also evident that the second (or right) peak, i.e., the shell resonance, is greatly affected by the interference of the additional gold core. Without the inner gold particle, the shell resonance occurs at 795 nm. For a gold core of 40-nm radius, the peak red shifts to 915 nm. With a 50-nm radius gold core, the peak extends to 1145 nm. This trend indicates that, by introducing a gold core, it is possible to achieve shell resonance at 1300 nm. It should be stated here that all the size parameters discussed in this figure, i.e., gold particle with tens nanometer, silica layer with a few to tens of nanometer thick, and gold layer thicker than 10 nm are all feasible to be synthesized in laboratories. Thus, Au-SiO₂-Au structured nanoshells should be useful as a potential agent for bioimaging.

Inspection of Fig. 6 further shows that during the resonance right shifting, the ratio of scattering to absorption changes as well. In Fig. 6(a), scattering is dominant. With the size of the gold core increasing, the multilayered nanoshell becomes more absorbing. Eventually, the absorption is more significant than scattering. This is consistent with [31]. From this viewpoint, Au-SiO₂-Au structured nanoshells are also excellent candidates for photothermal treatment, by which tumor tissue can be thermally destroyed.

Fig. 7 shows the spectra properties of Au-SiO₂-Au structured nanoshells with gold core radius fixed at 40 nm, silica layer fixed at 20-nm thick, while the thickness of gold layer is varied. It is apparent that a thinner gold shell results in a longer wavelength resonance. This is in agreement with that of conventional nanoshell.

C. Spectra Properties of Nanoshell With Five and Seven Layers

Encouraged by the difference between conventional nanoshell and three-layer nanoshell, we further examined the optical properties of nanoshells with multiple layers of more than three layers. Fig. 8(a) and (b) illustrates, respectively, the spectra of nanoshell with five layers, i.e., Au-SiO₂-Au-SiO₂-Au in water, and with seven layers, i.e., Au-SiO₂-Au-SiO₂-Au-SiO₂-Au. It can be seen from Fig. 8(a) that compared to

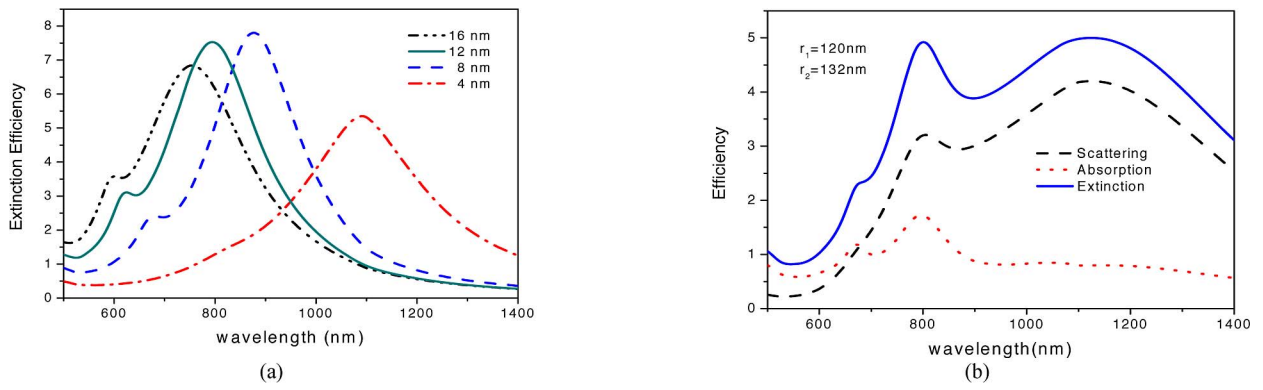


Fig. 5. Plasmon resonance variation with shell thickness. (a) Calculated extinction of Au-SiO₂ nanoshell with constant 60 nm radius core, while gold shell varies from 16 to 4 nm. (b). Extinction, absorption, and scattering spectra of an Au-SiO₂ nanoshell with 120-nm core radius and 12-nm shell thick. The surrounding medium is assumed as water in all the calculation.

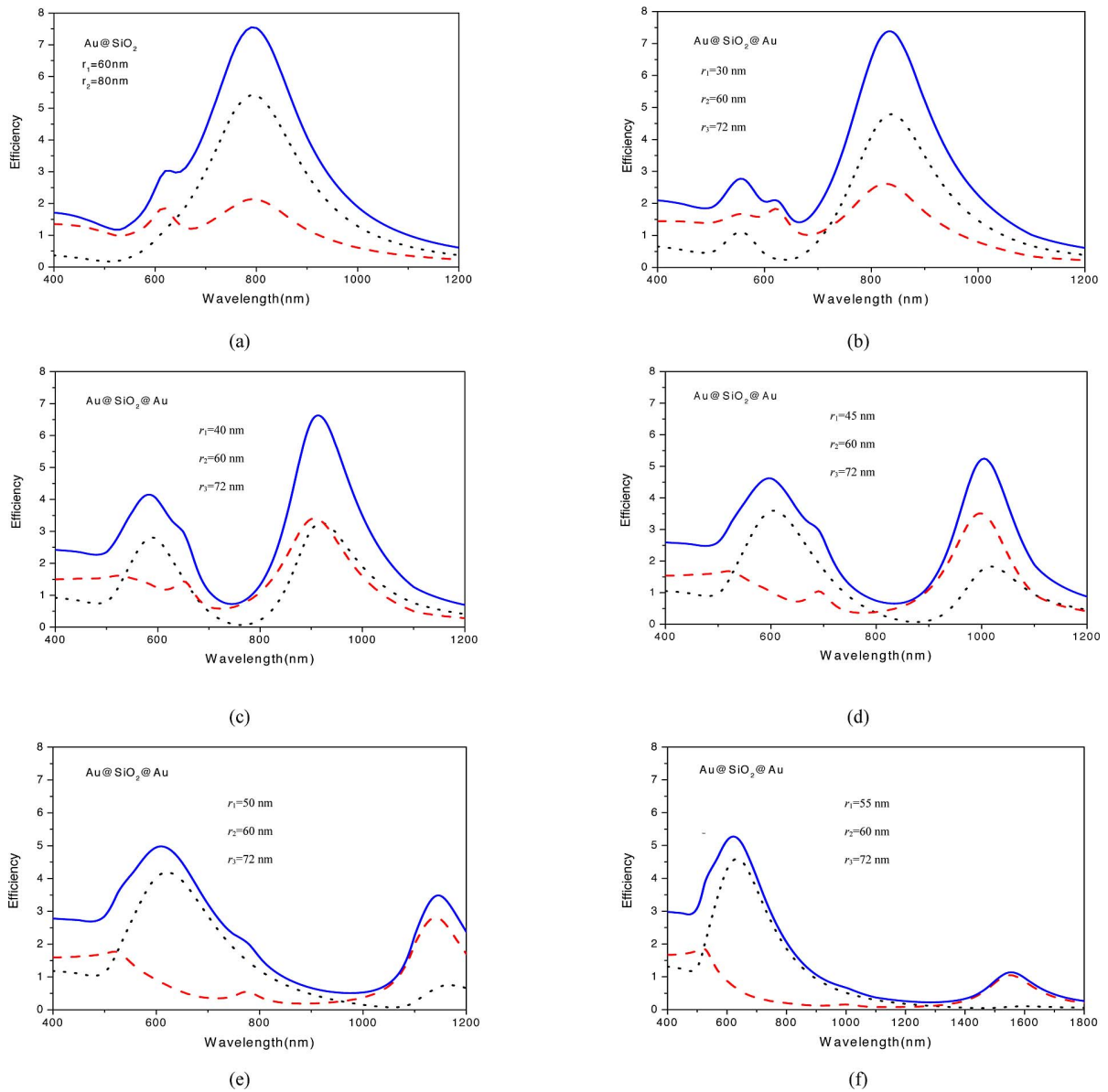


Fig. 6. Extinction, absorption, and scattering spectra of an Au-SiO₂-Au multilayered nanoshell. r_2 and r_3 are fixed at 60 and 72 nm, while the radius of inner gold particle varies. (a) r_1 is 0, i.e., the conventional Au-SiO₂ nanoshell. (b) $r_1 = 30$ nm, (c) $r_1 = 40$ nm, (d) $r_1 = 45$ nm, (e) $r_1 = 50$ nm, (f) $r_1 = 55$ nm. The solid, dotted, and dashed lines represent extinction, scattering, and absorption spectra, respectively.

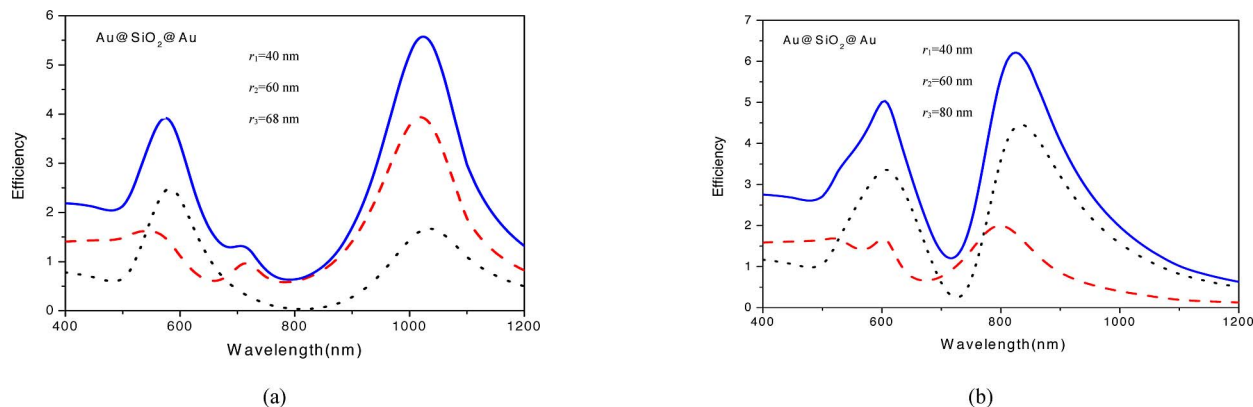


Fig. 7. Extinction, absorption, and scattering spectra of an Au-SiO₂-Au multilayered nanoshell. r_1 and r_2 are fixed to 40 and 60 nm, while the outer most shell thickness varies. (a) $\delta_3 = 8$ nm, and (b) $\delta_3 = 20$ nm. The solid line, dotted line, and dashed line represent extinction, scattering, and absorption spectra, respectively.

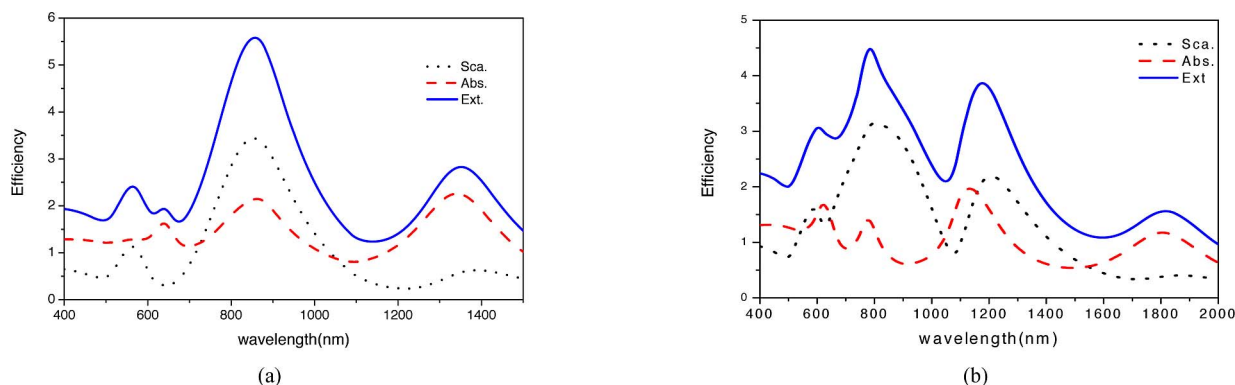


Fig. 8. Extinction, absorption, and scattering spectra of a nanoshell with multiple layers. (a) Five layer: Au-SiO₂-Au-SiO₂-Au with radii 30/50/60/80/90 nm (b) Seven layer: Au-SiO₂-Au-SiO₂-Au with radii 30/50/60/80/90/110/120 nm.

the Au-SiO₂-Au case, additional resonance peak appears in the NIR region. The peaks in Fig. 8(a), from left to right, are believed to be mainly contributed by the gold core, the middle gold layer, and the outmost gold layer, respectively. For the second peak, ~ 850 nm, the scattering is bigger than the absorption. For the third peak, ~ 1350 nm, however, it is just the opposite. In spite of the complex synthesis procedure of multilayer nanoshell, the phenomenon that two peaks with different scattering to absorption ratio in NIR hints us that such particles may be used as a bifunctional candidate for both bioimaging and photothermal treatment. The first NIR resonance peak with larger scattering efficiency is desired for OCT imaging, and the second NIR peak with larger absorption is more efficient to the thermal applications. Both functions are thus possibly realized by means of one type of nanoshell excited by two laser sources with reasonable frequencies, respectively. Confined to the length of the paper, detailed influencing factors, such as the core to shell ratio and the spacing dielectric media to the resonance properties, are not discussed here. It will be developed in our later study with the help of the presented algorithm.

Fig. 8(b) shows even more peaks in the NIR region. However, the fabrication of such multilayered nanoshells might be very complicated. The purpose of this figure is just to show the influencing trend of gold layers to the resonance. The potential application needs to be investigated further.

D. Near-Field Enhancement of a Multilayered Nanoshell

To reveal the nature of plasmon resonance of a multilayered nanoshell, the spatial distribution of electric-field enhancement in the vicinity of the nanoshell is investigated. The field enhancement was defined as (1). In Fig. 9, the contour plot was given for a conventional Au-SiO₂ nanoshell in water. Field enhancements are observed on both inside and outside surface of the gold shell. However, a stronger field appears in the vicinity of the outside than the inside of the nanoshell. Moreover, it is noticed that the maximum enhancement appears along the polarization direction (x -axis). This is due to the dominant dipole polarization produced by the polarized charges, which have a higher density at both upper end and lower end. In addition, the charges on the outer surface are much more than that on the inner surface [32], [33]. In Fig. 9(a), the enhancement slightly deviates from the exact polarization direction, which is contributed by the quadruple interaction effect. Since the size parameter in this case is more than 0.5, which is no longer a small particle for which higher order terms can be neglected.

Fig. 10 plots the field distributions inside and outside an Au-SiO₂-Au structured nanoshell. Only XOZ-plane was shown for analysis. The inner and outer radii of the gold shell are fixed at 60 and 72 nm, while the gold core varies from 30 to 45 nm. The corresponding thickness of the silica layer is 30,

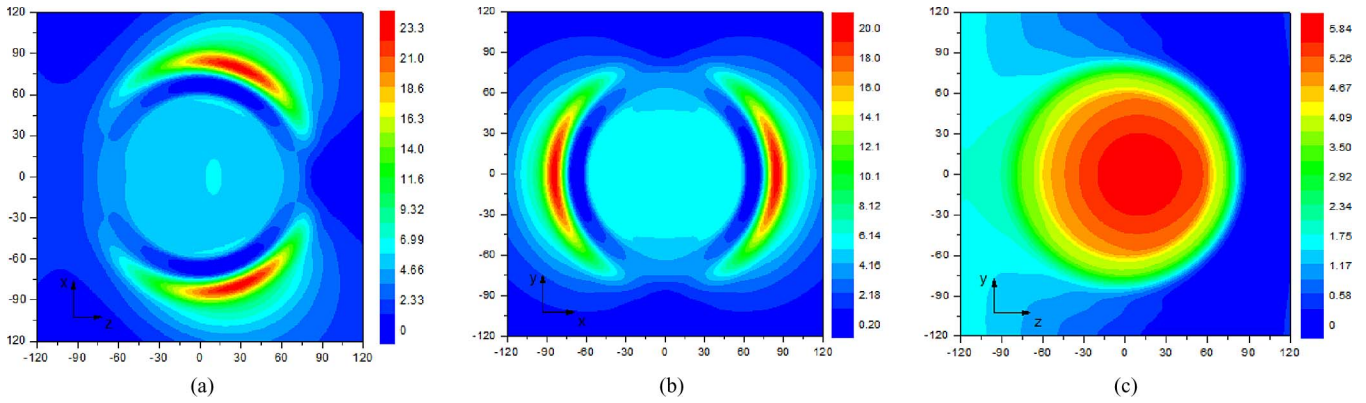


Fig. 9. Field enhancement in the vicinity of an isolated Au-SiO₂ nanoshell with 60-nm radius SiO₂ core and 12-nm thick gold layer. Wave propagates along z-axis, and field is polarized along x-axis. (a)–(c) are the three cross sections in planes indicated in the subtitles. (a) ZOx-plane. (b) XOY-plane. (c) ZOY-plane.

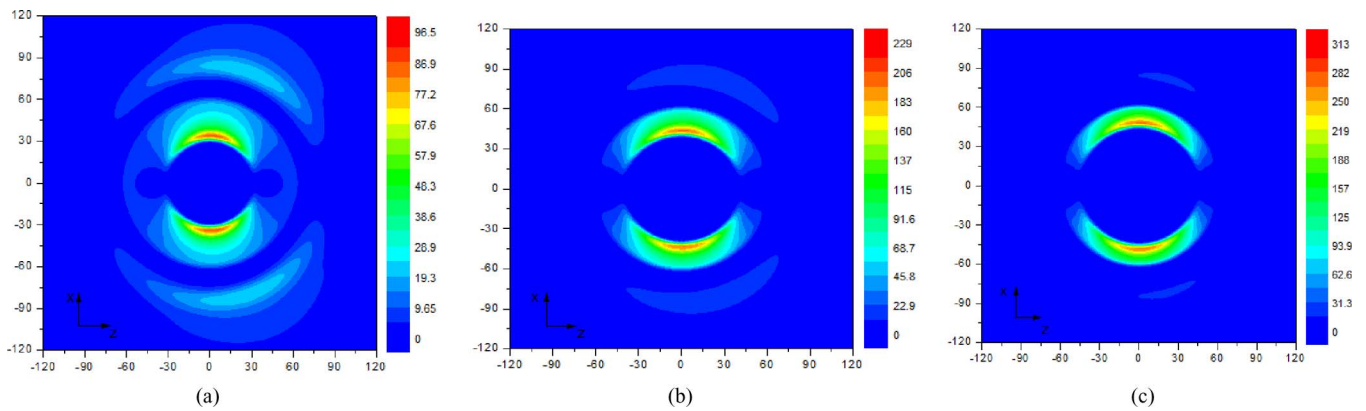


Fig. 10. Variation of field enhancement of an Au-SiO₂-Au nanoshell in XOZ cross section. The radii of $r_1/r_2/r_3$ are indicated in the subtitle. The corresponding wavelength for (a), (b), and (c) are 835, 915, and 1005 nm, respectively. (a) 30/60/72 nm. (b) 40/60/72 nm. (c) 45/60/72 nm.

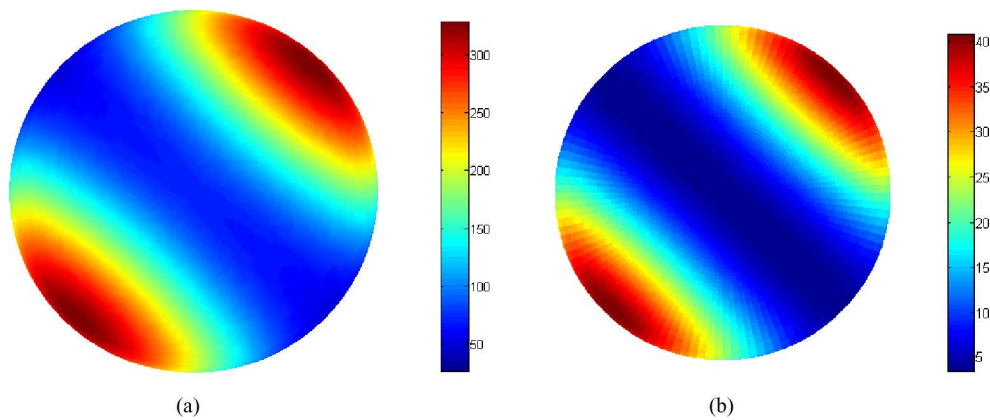


Fig. 11. Field enhancement at spherical surface, with $r_1/r_2/r_3 = 40/60/72$ nm. (a) $r = 50$ nm. (b) $r = 73$ nm.

20, and 15 nm, respectively, and the contours were plotted at resonance wavelengths of 835, 915, and 1005 nm for Fig. 9(a)–(c), respectively. It is seen that the maximum field is still along the polarization direction, however, it now occurs inside the dielectric layer instead outside. As shown in the figure, the narrower the space, the stronger the enhancement becomes. This can be explained by the reflecting and absorbing behavior of EM wave in a cavity. When incident light irradiates an Au-SiO₂-Au-structured nanoshell, a part of energy penetrates through

the outer metal shell and then propagates toward the inner gold particles. Between the two surfaces of r_1 and r_2 , light is reflected back and forth in the dielectric space, being trapped in the gap. With the space getting narrower, the back-forth reflection occurs more frequently. Furthermore, it is also noticed from Fig. 10 that the field enhancement in the vicinity of the outer most surface still keeps the asymmetric distribution caused by the motioned quadruple effect. In order to quantify the field enhancement, the contours at both inside and outside surface are plotted, as shown

in Fig. 11. Fig. 11(a) and (b) is the field enhancement at surface $r = 50$ and 73 nm, respectively. The former is inside the silica layer and the latter is outside the gold layer. It can be seen that except the magnitude difference, the contour distribution at the two locations are almost the same.

IV. CONCLUSION

In this paper, a multipole expansion model coupled with an efficient recursive algorithm was employed to investigate the surface plasmon resonance of a multilayered nanoshell. The model was first verified by the scattering spectra of a single Au-SiO₂ nanoshell, and then, applied to investigate the optical spectra of multilayered nanoshell for potential application in photothermal cancer treatment and biological imaging. After a series of theoretical calculation and analysis, the following conclusions can be made.

- 1) Compared with a single-layered Au-SiO₂ nanoshell, a multilayered nanoshell produces additional dipole peaks in the spectra. The number of peaks depends on the number of gold layers, and the peak positions are affected by the geometry size.
- 2) A three-layered gold nanoshell can shift the LSPR at wavelength of 1300 nm or even longer under the condition of feasible gold layer thickness and without much widening the line width.
- 3) A five-layered nanoshell can exhibit two resonance peaks in NIR region. Dual imaging/heating function may be realized by designing one peak with larger scattering and the other peak with larger absorption. The former is believed crucial for ultrahigh resolution OCT bioimaging, and the later is desired for high-efficiency thermal treatment.
- 4) The maximum field enhancement of an Au-SiO₂-Au nanoshell happens inside the silica layer. With other parameters kept constant, the narrower the silica layer, the stronger the field is enhanced.

REFERENCES

- [1] L. R. Hirsch, R. J. Stafford, and J. A. Bankson, S. R. Sershen, B. Rivera, R. E. Price, J. D. Hazle, N. J. Halas, and J. L. West, "Nanoshell-mediated near-infrared thermal therapy of tumors under magnetic resonance guidance," *Proc. Nat. Acad. Sci. (PNAS)*, vol. 100, no. 23, pp. 13549–13554, 2003.
- [2] D. P. O'Neal, L. R. Hirsch, and N. J. Halas, "Photo-thermal tumor ablation in mice using near infrared-absorbing nanoparticles," *Cancer Lett.*, vol. 209, no. 2, pp. 171–176, 2004.
- [3] C. Loo, L. Hirsch, and M. H. Lee, "Gold nanoshell bioconjugates for molecular imaging in living cells," *Opt. Lett.*, vol. 30, no. 9, pp. 1012–1014, 2005.
- [4] C. Loo, A. Lowery, N. J. Halas, J. L. West, and R. Drezek, "Immunotargeted nanoshells for integrated cancer imaging and therapy," *Nano Lett.*, vol. 5, no. 4, pp. 709–711, 2005.
- [5] A. M. Gobin, M. H. Lee, and N. J. Halas, "Near-infrared resonant nanoshells for combined optical imaging and photothermal cancer therapy," *Nano Lett.*, vol. 7, no. 7, pp. 1929–1934, 2007.
- [6] J. G. Fujimoto, M. E. Brezinski, G. T. Tearney, S. A. Boppart, B. E. Bouma, M. R. Hee, J. F. Southern, and E. A. Swanson, "Biomedical imaging and optical biopsy using optical coherence tomography," *Nature Med.*, vol. 1, no. 9, pp. 970–972, 1995.
- [7] H. K. Moon, S. H. Lee, and H. C. Choi, "In vivo near-infrared mediated tumor destruction by photothermal effect of carbon nanotubes," *Amer. Chem. Soc. (ACS) Nano*, vol. 3, no. 11, pp. 3707–3713, 2009.
- [8] S. L. Westcott, S. J. Oldenburg, T. R. Lee, and N. J. Halas, "Formation and adsorption of clusters of gold nanoparticles onto functionalized silica nanoparticle surfaces," *Langmuir*, vol. 14, no. 19, pp. 5396–5401, 1998.
- [9] T. Pham, J. B. Jackson, N. J. Halas, and T. R. Lee, "Preparation and characterization of gold nanoshells coated with self-assembled monolayers," *Langmuir*, vol. 18, no. 12, pp. 4915–4920, 2002.
- [10] R. Ashayer, S. H. Mannan, and S. Sajjadi, "Synthesis and characterization of gold nanoshells using poly(diallyldimethyl ammonium chloride)," *Colloids Surf. A: Physicochem. Eng. Aspects*, vol. 329, no. 3, pp. 134–141, 2008.
- [11] N. Phonthammachai, J. C. Kah, G. Jun, C. J. Sheppard, M. C. Olivo, S. G. Mhaisalkar, and T. J. White, "Synthesis of contiguous silica-gold core-shell structures: Critical parameters and processes," *Langmuir*, vol. 24, no. 9, pp. 5109–5112, 2008.
- [12] J. H. Kim, W. W. Bryan, and T. R. Lee, "Preparation, characterization, and optical properties of gold, silver, and gold-silver alloy nanoshells having silica cores," *Langmuir*, vol. 24, no. 19, pp. 11147–11152, 2008.
- [13] X. Xia, Y. Liu, V. Backman, and G. A. Ameer, "Engineering sub-100 nm multi-layer nanoshells," *Nanotechnology*, vol. 17, no. 21, pp. 5435–5440, 2006.
- [14] A. F. Fercher, W. Drexler, C. K. Hitzenberger, and T. Lasser, "Optical coherence tomography: Principles and applications," *Rep. Prog. Phys.*, vol. 66, no. 2, pp. 239–303, 2003.
- [15] K. Bizheva, A. Unterhuber, B. Hermann, B. Považay, H. Sattmann, and W. Drexler, "Imaging ex vivo and in vitro brain morphology in animal models with ultrahigh resolution optical coherence tomography," *J. Bio. Opt.*, vol. 9, no. 4, pp. 719–724, 2004.
- [16] W. Drexler, "Ultrahigh-resolution optical coherence tomography," *J. Bio. Opt.*, vol. 9, no. 1, pp. 47–74, 2004.
- [17] J. M. Schmitt, M. Yadlowsky, and R. F. Bonner, "Subsurface imaging of living skin with optical coherence tomography," *Dermatology*, vol. 191, pp. 93–98, 1995.
- [18] J. M. Schmitt and A. Knüttel, "Model of optical coherence tomography of heterogeneous tissue," *J. Opt. Soc. Amer. A*, vol. 14, no. 6, pp. 1231–1242, 1997.
- [19] E. Prodan, A. Lee, and P. Nordlander, "The effect of a dielectric core and embedding medium on the polarizability of metallic nanoshells," *Chem. Phys. Lett.*, vol. 360, no. 3–4, pp. 325–332, 2002.
- [20] S. J. Oldenburg, S. L. Westcott, R. D. Averitt, and N. J. Halas, "Surface enhanced Raman scattering in the near infrared using metal nanoshell substrates," *J. Chem. Phys.*, vol. 111, no. 10, pp. 4729–4735, 1999.
- [21] K. Chen, Y. Liu, G. Ameer, and V. Backman, "Optimal design of structured nanospheres for ultrasharp light-scattering resonances as molecular imaging multilabels," *J. Bio. Opt.*, vol. 10, no. 2, pp. 024005-1–024005-6, 2005.
- [22] A. L. Aden and M. Kerker, "Scattering of electromagnetic waves from two concentric spheres," *J. Appl. Phys.*, vol. 22, no. 10, pp. 1242–1246, 1951.
- [23] J. R. Wait, "Electromagnetic scattering from radially inhomogeneous spheres," *Appl. Sci. Res. B*, vol. 10, no. 5–6, pp. 441–450, 1963.
- [24] R. Bhandari, "Scattering coefficients for a multilayered sphere: Analytic expressions and algorithms," *Appl. Opt.*, vol. 24, no. 13, pp. 1960–1967, 1985.
- [25] C. F. Bohren and D. R. Huffman, *Absorption and scattering of light by small particles*. New York: Wiley, 1983.
- [26] D. W. Mackowski, R. A. Altenkirch, and M. P. Menguc, "Internal absorption cross sections in a stratified sphere," *Appl. Opt.*, vol. 29, no. 10, pp. 1551–1559, 1990.
- [27] Z. S. Wu and Y. P. Y. Wang, "Electromagnetic scattering for multilayered sphere: Recursive algorithms," *Radio Sci.*, vol. 26, no. 6, pp. 1393–1401, 1991.
- [28] W. Yang, "Improved recursive algorithm for light scattering by a multilayered sphere," *Appl. Opt.*, vol. 42, no. 9, pp. 1710–1720, 2003.
- [29] P. B. Johnson and R. W. Christy, "Optical constants of the noble metals," *Phys. Rev. B*, vol. 6, no. 12, pp. 4370–4379, 1972.
- [30] C. L. Nehl, N. K. Grady, G. P. Goodrich, F. Tam, N. J. Halas, and J. H. Hafner, "Scattering spectra of single gold nanoshells," *Nano Lett.*, vol. 4, no. 12, pp. 2355–2359, 2004.
- [31] Y. Hu, R. C. Fleming, and R. A. Drezek, "Optical properties of gold-silica-gold multilayer nanoshells," *Opt. Expr.*, vol. 16, no. 24, pp. 19579–19591, 2008.
- [32] T. Okamoto, "Near-field spectral analysis of metallic beads," in *Near-Field Optics and Surface Plasmon Polaritons*, *Topics Appl. Phys.*, vol. 81, pp. 97–123, 2001.
- [33] E. Hao, S. Y. Li, R. C. Bailey, S. I. Zou, G. C. Schatz, and J. T. Hupp, "Optical properties of metal nanoshells," *J. Phys. Chem. B*, vol. 108, no. 4, pp. 1224–1229, 2004.



Changhong Liu received the B.S. degree from the Hefei University of Technology, Hefei, Anhui, China, in 1992, the M.S. degree from Tsinghua University, Beijing, China, in 2001, and Ph.D. degree from Shanghai Jiao Tong University, Shanghai, China, in 2009, all in electrical engineering.

From 2007 to 2009, she was Ph.D. degree Research Scholar at the University of Michigan-Dearborn, Dearborn. She is currently an Associate Professor at Shanghai Jiao Tong University. Her research interests include electromagnetic field, heat

transfer, and cooling technology.



Chris Chungting Mi (S'00–A'01–M'01–SM'03) received the B.S.E.E. and M.S.E.E. degrees from the Northwestern Polytechnical University, Xi'an, Shaanxi, China, and the Ph.D. degree from the University of Toronto, ON, Canada, all in electrical engineering.

From 2000 to 2001, he was an Electrical Engineer with General Electric Canada, Inc., where he was engaged in designing and developing large electric motors and generators up to 30 MW. He was also at the Rare-Earth Permanent Magnet Machine Institute,

Northwestern Polytechnical University. In 1994, he joined Xi'an Petroleum Institute as an Associate Professor and an Associate Chair of the Department of Automation. From 1996 to 1997, he was a Visiting Scientist at the University of Toronto. He is currently an Associate Professor and the Director of the Data Terminal Equipment (DTE) Power Electronics and Electrical Drives Laboratory, Department of Electrical and Computer Engineering, University of Michigan-Dearborn, Dearborn. He is the author or coauthor of more than 80 articles on the subject of electric machines, power electronics, and electric and hybrid vehicles. His current research interests include electric drives, power electronics, electric machines, renewable energy systems, and electrical and hybrid vehicles.

Dr. Mi is the Chair of the IEEE Southeastern Michigan Section from 2008 to 2009. He was the Vice Chair of the Section from 2006 to 2007. He is the recipient of the National Innovation Award, the Government Special Allowance Award, and the Distinguished Teaching Award of the University of Michigan-Dearborn. He is also the recipient of the 2007 IEEE Region 4 Outstanding Engineer Award, the IEEE Southeastern Michigan Section Outstanding Professional Award, and the Society of Automotive Engineers' Environmental Excellence in Transportation Award.



Ben Q. Li received the B.S. degree from the Central University, Hunan, China, in 1982, the M.S. degree from the Colorado School of Mines, Golden, in 1984, and the Ph.D. degree from the University of California, Berkeley, in 1989, all in mechanical engineering.

He was a Research Associate at the Massachusetts Institute of Technology, Cambridge, for about a year, and a Senior Engineer at Aluminum Company of America (Alcoa) for three years. He is currently a Professor and the Chair of the Department of Me-

chanical Engineering, University of Michigan-Dearborn, Dearborn. He is also the author or coauthor of more than 200 technical papers in archive journals and conference proceedings, and the author of one book and edited two books. He has been an invited keynote speaker at many domestic and international conferences. His research work has been supported by various federal National Science Foundation, National Aeronautics and Space Administration, Department of Energy, Department of Defense, the National Institute of Standards and Technology, and state agencies as well as private industries. His current research interests include the study of electromagnetics, fluid flow, and heat transfer in thermal-fluid systems.

Prof. Li is a Fellow of the American Society for Mechanical Engineers.